frontiers | Frontiers in Physics

TYPE Original Research
PUBLISHED 14 August 2023
DOI 10.3389/fphy.2023.1238101

OPEN ACCESS

EDITED BY
Xinzhong Li,
Henan University of Science and Technology, China

REVIEWED BY
Yuxuan Ren,
Fudan University, China
Chaoliang Ding,
Luoyang Normal University, China

*CORRESPONDENCE
Lixin Guo,
lxguo@xidian.edu.cn
Mingjian Cheng,
mjcheng@xidian.edu.cn

RECEIVED 10 June 2023
ACCEPTED 31 July 2023
PUBLISHED 14 August 2023

CITATION
Al-Ahsab HT, Cheng Q, Cheng M, Guo L, Cao Y and Wang S (2023), Propagation behavior of orbital angular momentum in vector anomalous vortex beams under maritime atmospheric turbulence. *Front. Phys.* 11:1238101. doi: 10.3389/fphy.2023.1238101

Propagation behavior of orbital angular momentum in vector anomalous vortex beams under maritime atmospheric turbulence

Hassan T. Al-Ahsab[1,2], Qi Cheng[3], Mingjian Cheng[1]*, Lixin Guo[1]*, Yuancong Cao[1] and ShuaiLing Wang[4]

[1]School of Physics, Xidian University, Xi'an, China, [2]Physics Department, Faculty of Applied Science, Thamar University, Thamar, Yemen, [3]504th Institute of China Aerospace Science and Industry Corporation (CASIC), Xi'an, China, [4]School of Physics Science and Engineering, Tongji University, Shanghai, China

This study explores the propagation properties of orbital angular momentum (OAM) carried by a vector anomalous vortex beam (VAVB) in maritime atmospheric turbulence, utilizing the Rytov approximation. A comparative analysis is conducted between the VAVB and Laguerre-Gaussian beam, revealing that the VAVB exhibits a higher detection probability under specific circumstances. This suggests that the VAVB is more suitable for scenarios where maximizing detection probability is critical. The detection probability of the signal OAM mode is affected by the characteristics of maritime atmospheric turbulence and propagation distance, but can be significantly improved by manipulating beam parameters such as wavelength, beam order, beam waist, and quantum number, while considering the characteristics of maritime atmospheric turbulence. Hence, the use of VAVB has the potential to facilitate reliable optical communication in challenging maritime environments.

KEYWORDS

orbital angular momentum, anomalous vortex beam, maritime atmospheric turbulence, detection probability, Rytov approximation

1 Introduction

Free-space communication systems using laser beam, also known as lasercom, have garnered significant interest due to the growing demand for high data transmission rates in various applications, including satellite communications for downlink/uplink, 6G communication links, and connections between buildings where fiber optics are not suitable [1]; [2]; [3]; [4]. However, the propagation of laser beams through turbulent media is greatly affected by the fluctuations in refractive index, resulting in beam spreading, beam wander, irradiance fluctuation, angle-of-arrival fluctuations, loss of spatial coherence, and random phase fluctuations [1]; [5]; [6]; [7]; [8]; [9]. Several methods have been employed to overcome these detrimental effects of turbulence, such as phase correction using adaptive optics, increasing the receiver aperture size, and utilizing partially coherent or vector beams [10]; [11]; [12]; [13]; [14]. It has been observed that vector beams are more resilient to turbulence compared to scalar ones, mitigating the turbulent effects and reducing the spreading of orbital angular momentum (OAM) spectrum [11]; [12]; [13]; [14].

The behavior of laser beam propagation in the marine environment differs from terrestrial atmospheric turbulence due to factors such as high humidity, temperature

fluctuations, irregular movement of seawater, changes in wind velocity, and their interactions [6]; [15]; [16]; [8]. Experimental data obtained over the Salton Sea has shown significant amplification of characteristic turbulence features of marine turbulence when compared to terrestrial atmospheric refractive spectra [17]; [18]. C. Jellen et al. have experimentally confirmed that the refractive index structure constant varies with respect to the time and depends on other turbulence parameters such as water-air temperature difference and pressure [19].

Various vortex beams, including Laguerre–Gaussian beams, Bessel–Gaussian vortex beams, hollow Gaussian vortex beams, and Airy vortex beams, have been generated in laboratories and extensively studied [16]; [20]; [21]; [22]; [23]; [24]; [25]; [26]; [27]; [28]; [29]. The OAM spectrum of Laguerre–Gaussian beams, Airy beams, Hankel–Bessel beams, and modified Bessel–Gaussian beams in the maritime atmospheric turbulence has been theoretically investigated based on the Rytov method [20]; [16,30]; [21]. Anomalous vortex beams (AVBs), a recent model of vortex beams, offer several advantages that make them promising for diverse applications [22]; [23]; [31]; [25]; [32]; [24]; [26]; [27]; [28]; [29]. AVBs can be generated in the laboratory using spatial light modulator [22]; [31]. Additionally, circularly polarized AVBs can be employed to generate Airy vortex beams [32], trap particles [26]; [27], facilitate lidar detection, and enable imaging in strong turbulent atmospheres [29]. Z. Dai discovered that the beam width of AVBs propagating through strongly nonlocal nonlinear media can remain invariant and periodically compressed or broadened [24]. Furthermore, it has been demonstrated that the spiral spectrum of scalar AVBs in weak atmospheric turbulence retains more power and carries a larger information capacity than scalar Laguerre–Gaussian beams [28]. The propagation characteristics of AVB beams through atmospheric turbulence depend on turbulence parameters, topological charge, and beam order [23]; [28]; [29]. In some cases, it has been observed that the spiral spectrum of partially coherent AVBs is higher than that of partially coherent Laguerre-Gaussian beams [23]. However, the propagation model of vector anomalous vortex beams (VAVBs) and their OAM modes require further investigation to develop an efficient model for carrying OAM mode for optical communication in maritime atmospheric turbulence.

In this paper, we investigate the propagation properties of VAVBs in maritime atmospheric turbulence using the multiple phase screen method. We also examine the detection probability of OAM of optical communication links utilizing VAVBs based on the Rytov approximation. In Section 2, we present a theoretical method for calculating the detection probability. In Section 3, we provide numerical simulations of the intensity distribution of VAVBs in maritime atmospheric turbulence, as well as the detection probability under different beam and turbulence parameters. Finally, we summarize our findings and present a conclusion in Section 4.

2 Theoretical model

In cylindrical coordinate system (r, ϕ, z), the initial electric field of the vector anomalous vortex beam at the source plane $z = 0$ can be expressed as two perpendicular scalar components vortex beams in x and y directions as follows [33]:

$$\mathbf{E}_s^i(r,\varphi,\quad z=0) = E_{s,AV}^i(r,0)\begin{bmatrix}\cos(s\varphi+\varphi_0)\\ \sin(s\varphi+\varphi_0)\end{bmatrix}, \tag{1}$$

where s is the topological charge or quantum number of the beam which may take either positive or negative integer values, ϕ_0 is the initial phase angle that gives radial and azimuthal polarization for 0 and $\pi/2$, respectively. The electric field $E_{s,AV}^i(r,\phi,0)$ of the anomalous vortex beam is expressed as [22].

$$E_{s,AV}^i(r,0) = E_0\exp\left[-\frac{r^2}{w_0^2}\right]\left(\frac{r}{w_0}\right)^{2n+|s|}, \tag{2}$$

where E_0 is a constant, w_0 is the beam waist radius of the fundamental Gaussian beam and n is the beam order. This equation can be reduced to a Gaussian beam when $n = s = 0$, a hollow Gaussian beam when $n \neq 0$ and $s = 0$, Gaussian vortex beam when $n = 0$ and $s \neq 0$.

Under the paraxial approximation, the electric field of anomalous vortex beam propagated in free space at distance z from the source plane, based on the Huygens–Fresnel integral, can be given as [22]:

$$E_{s,AV}^{free}(\rho,\varphi,z) = f_{AV}(\rho,z)\exp(-is\varphi), \tag{3}$$

with

$$f_{AV}(\rho,z) = \frac{i^{s+1}\pi E_0 n!}{\lambda z G^{n+|s|+1}}\exp\left[-\frac{ik}{2z}\rho^2 - ikz\right]\left(\frac{k\rho}{2z}\right)^{|s|}L_n^{|s|}\left[\frac{k^2\rho^2}{4Gz^2}\right]\exp\left[-\frac{k^2\rho^2}{4Gz^2}\right], \tag{4}$$

where $k = \frac{2\pi}{\lambda}$ is the wave number with wavelength λ, $L_n^{|s|}$ is the associated Laguerre polynomial and $G = \frac{1}{w_0^2} + \frac{ik}{2z}$. The last equation should be multiplied by $(-1)^s$for $s < 0$. To clearly understand the propagation properties of AVB in free-space, the normalized intensity distribution is illustrated in Figure 1. AVB is a type of laser beam with self-focusing properties, which means that AVB can focus itself without the need for external optical components like lenses. The self-focusing point of AVB can be controlled by adjusting its beam parameters such as topological charge (OAM) and beam order. The medium through which the beam is propagating can also affect the self-focusing point.

The two components of VAVB in free space can be decomposed into positive and negative vortex beams that encoded into a right circularly polarized and left circularly polarized beams, respectively, with equal intensity and opposite spiral phases as follows.

$$E_{s,x}^{free}(\rho,\phi,z) = \frac{1}{2}f_{AV}(\rho,z)\left[\exp(is\phi+i\phi_0) + \exp(-is\phi-i\phi_0)\right] \tag{5}$$

$$E_{s,y}^{free}(\rho,\phi,z) = -i\frac{1}{2}f_{AV}(\rho,z)\left[\exp(is\phi+i\phi_0) - \exp(-is\phi-i\phi_0)\right]. \tag{6}$$

In turbulent mediums the intensity distribution and phase of the beam are distorted. Based on the Rytov approximation, the propagated electric field of the vector vortex beams in turbulence can be treated similarly to scalar vortex beams [34]; [11]. Therefore, the x-polarized component of electric field for VAVB after propagating through maritime atmospheric turbulence at the receiver plane can be expressed as [5].

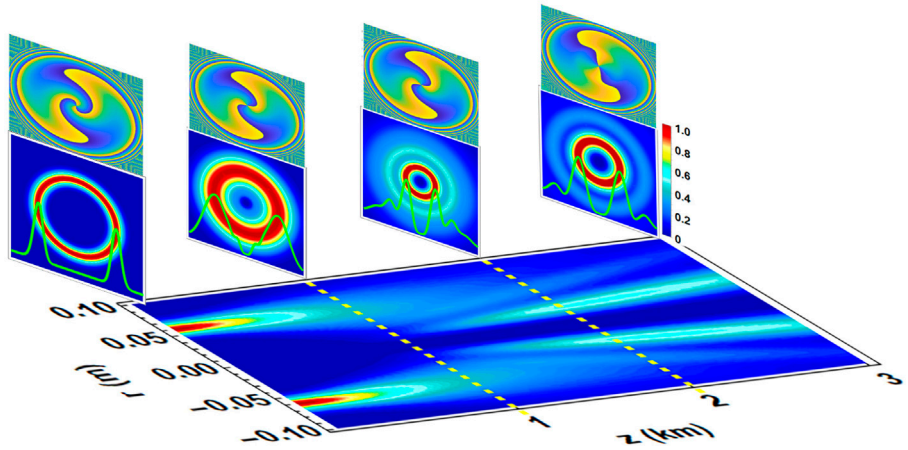

FIGURE 1
Normalized longitudinal intensity distribution, transverse normalized intensity and phase diagrams at z = 0, 1,2 and 3 *km* of scalar anomalous vortex beam propagated in free space with parameters n = 8, s = 2, w_0 =0.02 m and λ = 1550 *nm*.

$$E_{s,x}(\rho,\varphi,z) = E_{s,x}^{free}(\rho,\varphi,z)\exp[\psi(\rho,\varphi,z)], \tag{7}$$

where $\psi(\rho, \varphi, z)$ is the phase perturbation of the propagated beam through maritime atmospheric turbulence. The complex amplitude of VAVB disturb due to the refractive index fluctuations of the turbulence causing spreading of OAM to neighboring states. Based on the method of Fourier series expansion and the superposition theory of the spiral harmonics, the received electric field of VAVB can be expressed as [35].

$$E_{s,x}(\rho,\varphi,z) = \frac{1}{\sqrt{2\pi}}\sum_{m=-\infty}^{\infty} a_{m,x}(\rho,z)\exp(im\varphi), \tag{8}$$

where $a_{m,x}(\rho, z)$ is the Fourier coefficients, that can be obtained by Fourier inversion as

$$a_{m,x}(\rho,z) = \frac{1}{\sqrt{2\pi}}\int_0^{2\pi} E_{s,x}(\rho,\varphi,z)\exp(-im\varphi)d\varphi, \tag{9}$$

Now, the probability density distribution with mode m of VAVB in the paraxial channel can be given as

$$\langle|a_{m,x}(r,z)|^2\rangle = \frac{1}{2\pi}\int_0^{2\pi}\int_0^{2\pi} E_{s,x}(\rho,\varphi,z)E_{s,x}^{\star}(\rho',\varphi',z) \times[\exp(-im(\varphi-\varphi'))]d\varphi d\varphi', \tag{10}$$

where $\langle.\rangle$ is the ensemble average and the asterisk represents the complex conjugate. Substituting Eq. 7 into Eq. 10

$$\langle|a_{m,x}(r,z)|^2\rangle = \frac{1}{2\pi}\int_0^{2\pi}\int_0^{2\pi} E_{s,x}^{free}(\rho,\varphi,z)E_{s,x}^{free^{\star}}(\rho',\varphi',z) \times\langle\exp[\psi(\rho,\varphi,z)+\psi^{\star}(\rho',\varphi',z)]\rangle\exp(-im(\varphi-\varphi'))d\varphi d\varphi'. \tag{11}$$

Based on the quadratic approximation of the wave structure function, the mid term in the last formula, the phase correlation function can be given as

$$\exp[\psi(\rho,\varphi,z)+\psi^{*}(\rho,\varphi,z)] = \exp\left[-\frac{2\rho^2-2\rho^2\cos(\varphi-\varphi')}{\rho_0^2}\right], \tag{12}$$

where ρ_0 represents the coherence length of a spherical wave propagating through non-Kolmogorov maritime atmospheric turbulence that is given by [15]; [30]; [36].

$$\rho_0 = \left[\frac{\pi^2}{3}k^2 z\int_0^{\infty}\kappa^3\Phi_n(\kappa)d\kappa\right]^{-1/2}, \tag{13}$$

since $\Phi_n(\kappa)$ is the power spectrum of refractive-index fluctuations in non-kolmogrov and isotropic maritime atmospheric turbulence with $\kappa = \sqrt{\kappa_x^2+\kappa_y^2}$, that is expressed as [5].

$$\Phi_n(\kappa) = A(\alpha)\tilde{C}_n^2\left[1+a_1\frac{\kappa}{\kappa_H}+a_2\left(\frac{\kappa}{\kappa_H}\right)^{3-\alpha/2}\right]\frac{\exp[-\kappa^2/\kappa_H^2]}{(\kappa^2+\kappa_0^2)^{\alpha/2}}, \tag{14}$$

where $A(\alpha) = \Gamma(\alpha - 1)\cos(\pi\alpha/2)/(4\pi^2)$; α is the non-Kolmogrov parameter; $\tilde{C}_n^2$ in unit $m^{3-\alpha}$ is the generalized refractive index structure constant that can be reduced to the structure constant with units $m^{2/3}$ when α = 11/3; (a_1, a_2) = (−0.061, 2.836) and (1.802, −0.254) for maritime atmospheric turbulence and terrestrial turbulence, respectively; $\kappa_0 = 2\pi/L_0$ with outer scale of turbulence L_0; $\kappa_H = c(\alpha)/l_0$ with inner scale of turbulence l_0; and $c(\alpha)$ is expressed as [30].

$$c(\alpha) = \left(\pi A(\alpha)\left[\Gamma\left(\frac{3-\alpha}{2}\right)\left(\frac{3-\alpha}{3}\right)+a_1\Gamma\left(\frac{4-\alpha}{2}\right)\left(\frac{4-\alpha}{3}\right) + a_2\Gamma\left(\frac{12-3\alpha}{4}\right)\left(\frac{4-\alpha}{2}\right)\right]\right)^{1/(\alpha-5)}. \tag{15}$$

Substitute Eq. 14 into Eq. 13 and use the integral form of the second kind of a hypergeometric function $U(p; q; x)$ that is defined as follows [37].

$$\int_0^{\infty}\exp(-xt)t^{p-1}(1+t)^{q-p-1}dt = \Gamma(p)U(p;q;x) \quad ; \quad p>0. \tag{16}$$

The spatial coherence length can be expressed as

$$\rho_0^{-2} = \frac{\pi^2}{6}k^2 zA(\alpha)\tilde{C}_n^2\left[\kappa_0^{4-\alpha}U\left(2;\frac{6-\alpha}{2};\frac{\kappa_0^2}{\kappa_H^2}\right)+\frac{a_1}{\kappa_H}\kappa_0^{5-\alpha}\Gamma\left(\frac{5}{2}\right)U\left(\frac{5}{2};\frac{7-\alpha}{2};\frac{\kappa_0^2}{\kappa_H^2}\right) + \frac{a_2}{\kappa_H^{(6-\alpha)/2}}\kappa_0^{(14-3\alpha)/2}\Gamma\left(\frac{14-\alpha}{4}\right)U\left(\frac{14-\alpha}{4};\frac{18-3\alpha}{4};\frac{\kappa_0^2}{\kappa_H^2}\right)\right], \tag{17}$$

The probability of the OAM mode with quantum number s of VAVB after propagating in the maritime atmospheric turbulence of the x-polarized electric field component can be expressed as

$$P_x(s) = \iint \langle |a_s(r,z)|^2 \rangle \rho\rho' d\rho d\rho'. \tag{18}$$

Substituting Eqs 5, 11, 12 into Eq. 18, the probability density distribution of OAM modes of VAVB in the case of $x-$ polarization direction can be obtained as

$$\begin{aligned} P_x(s) = \frac{1}{2\pi}\iiint_0^{2\pi}\int_0^{2\pi} f(\rho,z) f^*(\rho,z) \exp\left[\frac{2\rho^2\cos(\varphi-\varphi')}{\rho_0^2}\right] \\ \times \left[\exp\left[i(s-m)(\varphi-\varphi')\right]\right. \\ + \exp\left[-i(s+m)\varphi - i(s-m)\varphi'\right]\exp\left[-2i\varphi_0\right] \\ + \exp\left[i(s-m)\varphi + i(s+m)\varphi'\right] \\ \left.\times \exp\left[2i\varphi_0\right] + \exp\left[-i(s+m)(\varphi-\varphi')\right]\right]\rho\rho' d\rho d\rho' d\varphi d\varphi'. \end{aligned} \tag{19}$$

Based on the orthogonality of OAM mode and using following integral formulae Gradshteyn and Ryzhik [38].

$$\int_0^{2\pi} \exp\left[-il\varphi + \eta\cos(\varphi-\varphi')\right]d\varphi = 2\pi\exp\left[-in\varphi'\right]I_l(\eta), \tag{20}$$

$$\int_0^{2\pi} \exp\left[-il\varphi\right]d\varphi = \begin{cases} 2\pi & ; l = 0 \\ 0 & ; l \neq 0, \end{cases} \tag{21}$$

Where$I_n(\eta)$ is the modified Bessel function of the first kind of order l, we conclude

$$\begin{aligned} P_x(s) = \frac{2\pi}{|G|^{2(n+|s|+1)}}\left(\frac{\pi E_0 n!}{\lambda z}\right)^2 \int_0^{d/2} \exp\left[-\frac{2\rho^2}{\rho_0^2}\right]\left(\frac{k\rho}{2z}\right)^{2|s|}\left|\exp\left[-\frac{k^2\rho^2}{4Gz^2}\right]L_n^{|s|}\left[\frac{k^2\rho^2}{4Gz^2}\right]\right|^2 \\ \times \left[I_{s-m}\left(\frac{2\rho^2}{\rho_0^2}\right) + I_{s+m}\left(\frac{2\rho^2}{\rho_0^2}\right)\right]\rho d\rho \end{aligned} \tag{22}$$

where d is the diameter of receiving aperture. With same procedure the detection probability of OAM mode for Laguerre–Gaussian beam of order n and quantum number s is given as

$$\begin{aligned} P_x(s) = \frac{n! w_0^2}{4\pi^2(n+|s|)! w^2(z)}\int_0^{d/2} \exp\left[-\frac{2\rho^2}{\rho_0^2}\right]\left(\frac{\sqrt{2}\rho}{w(z)}\right)^{2|s|}\left|\exp\left[-\frac{\rho^2}{w^2(z)}\right]L_n^s\left[\frac{2\rho^2}{w^2(z)}\right]\right|^2 \\ \times \left[I_{s-m}\left(\frac{2\rho^2}{\rho_0^2}\right) + I_{s+m}\left(\frac{2\rho^2}{\rho_0^2}\right)\right]\rho d\rho, \end{aligned} \tag{23}$$

where $w(z) = w_0\sqrt{1+(z/z_R)}$ and $z_R = kw_0^2/2$ represents the Rayleigh range. Herein, the electric field through free space of Laguerre-Gaussian beam is expressed as

$$E_{s,LG}^{free}(\rho,\varphi,z) = f_{LG}(\rho,z)\begin{bmatrix}\cos(s\varphi+\varphi_0)\\ \sin(s\varphi+\varphi_0)\end{bmatrix},$$

where

$$\begin{aligned} f_{LG}(\rho,z) = \frac{w_0}{w(z)}\sqrt{\frac{n!}{\pi(n!+|s|)!}}L_n^s\left[\frac{2\rho^2}{w^2(z)}\right]\exp\left[ikz - i(2n+|s|+1)\tan^{-1}\left(\frac{z}{z_R}\right)\right] \\ \times \left(\frac{\sqrt{2}\rho}{w(z)}\right)^n \exp\left(\frac{\rho^2}{w^2(z)} - \frac{ikz\rho^2}{2(z^2+z_R^2)}\right), \end{aligned}$$

At the receiver plane, the normalized detected probability of a signal OAM mode with quantum number s for the VAVB of order n after propagating in maritime atmospheric turbulence can be expressed as

$$P_x(m|s) = \frac{P_x(m)}{\sum_{m=0}^{\infty} P_x(m)}. \tag{24}$$

The mode probabilities of the OAM carried by VAVB in the x and y polarization directions have to detect independently and separately in order to measure the opposite signs of OAM modes and treated as a positive modes for both cases $-s$ and $+s$. Therefore, the detection probability of s mode can be express as Yuan et al. [34]; Cheng et al. [11].

$$P(m|s) = P_x(m|s) + P_y(m|s) = 2P_x(m|s). \tag{25}$$

3 Numerical analysis and discussion

In this section, the intensity distribution of the propagated VAVB through maritime atmospheric turbulence is discussed based on the multiple phase screen method [11]. After that, the numerical results for the OAM spectrum and received power or OAM mode detection probability are presented and discussed based on Eqs. (22)-25). The simulation parameters are $E_0 = 1$, $\lambda = 1.55\ \mu m$, $w_0 = 0.02$ m, $s = m = 3$, $n = 3$, $d = 0.20$ m, the distance between two phase screens $\triangle z$ is 10 m with grid 512 × 512, $\alpha = 11/3$, $C_n^2 = 1\times10^{-15}$, $z = 1$ km, $L_0 = 10$ m, and $l_0 = 5$ mm unless otherwise specified.

To better understand the propagation characteristics of OAM carried by the VAVBs in maritime atmospheric turbulence, we first demonstrate the evolution of intensity distribution through free space and through maritime atmospheric turbulence. Figure 2 compares the normalized intensity distributions of propagated VAVBs and vector Laguerre-Gaussian vortex beams (VLGBs) in free space and maritime atmospheric turbulence, with different values of beam order (n = 1, 3, and 4) and quantum number (s = 1 and 4) at four different propagation distances (z = 0 m, 1,000 m, 2000 m, and 3,000 m). As shown in Figure 2, it can be seen that both VAVBs and VLGBs are vector beam types capable of carrying OAM, which enables them to maintain their shape and hollow intensity profile over long distances. However, when these beams propagate through atmospheric turbulence, they are subject to various effects caused by random fluctuations in the refractive index of the medium. These effects include beam spreading, scintillation, and wavefront distortion, which can cause the vortex beam to lose its hollow profile, and increase the size of the dark spot at the center of the beam as the distance of propagation increases. It is important to note that the specific effects may vary depending on the properties of the beam and the turbulence conditions. One significant difference between VAVBs and LG beams is their phase structure. LG beams have a singular helical phase front, whereas VAVB beams exhibit a more intricate phase structure around the singularities, featuring higher-order helicoidal structures. This complex phase structure allows VAVBs to be less susceptible to distortion and spreading under long-distance turbulent conditions compared to LG beams. Furthermore, VAVBs with high quantum numbers have a larger hollow size, which indicates that the diffraction and turbulence effects on the propagated beam are more significant. As a result, the intensity distribution of VAVBs with high beam orders may be more distorted than those with low beam orders. However, the self-focusing property of VAVBs becomes more pronounced with increasing beam order, which can counteract the distortions in the beam

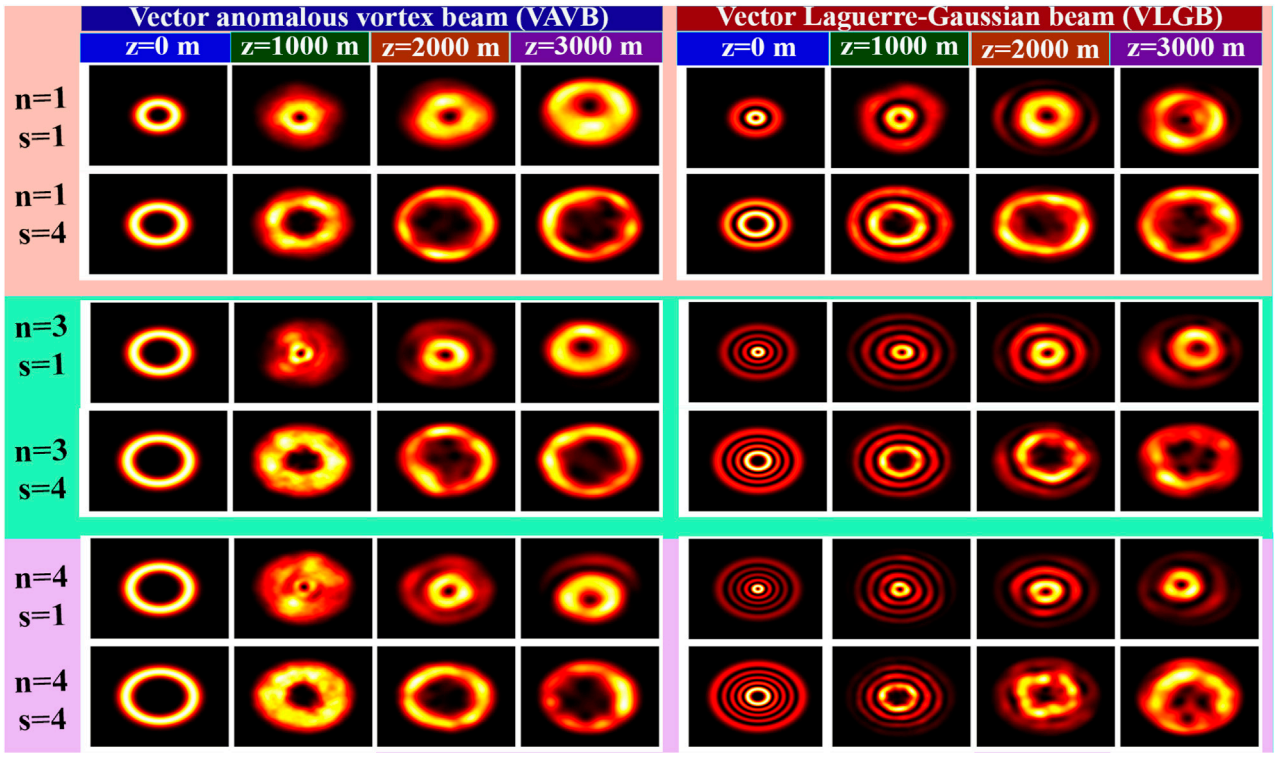

FIGURE 2
Intensity distribution of vector anomalous vortex beam and vector Laguerre-Gaussian beam propagated in maritime atmospheric turbulence.

profile during long-distance propagation. In summary, the propagation of VAVBs through a medium with atmospheric turbulence is a complex phenomenon that depends on several parameters, including the beam order, quantum number, and propagation distance. Understanding these effects is crucial for optimizing the performance of OAM carried by VAVBs in various applications.

Figure 3 shows the comparison of the detection probabilities of the signal OAM mode for VAVBs and VLGBs propagated through maritime atmospheric turbulence, as a function of beam order *n* and quantum number *s*. At short distances, both VAVBs and VLGBs with lower beam orders and quantum numbers exhibit higher detection probabilities for the signal OAM mode. The increase in beam size with increasing beam order and quantum number leads to more diffraction and turbulence effects, resulting in a reduction of the signal OAM detection probability, particularly for VLGBs. This reduction becomes more pronounced at high quantum numbers. However, at longer distances, the situation reverses for VAVBs, with higher beam orders demonstrating higher detection probabilities compared to lower-order VAVBs. This reversal can be attributed to the self-focusing property of VAVBs, which becomes more pronounced for high beam orders. As a result, for distances smaller than 700 m, the signal OAM mode detection probabilities of VAVBs for all values of *s* are higher than those of VLGBs, using the parameters mentioned earlier. It is worth noting that VAVBs are only superior in short distances with small beam orders. For large propagation distances, VLGBs may be more suitable than VAVBs. Therefore, the choice of which type of beam to use depends on the specific application and the required propagation distance.

Figure 4 illustrates the detection probability of VAVB's signal OAM mode with different beam waist and wavelength. It is shown that both the beam waist and wavelength affect the detection probability of VAVB's signal OAM mode, with the beam waist becoming the dominant factor at longer propagation distances. A larger beam waist helps minimize diffraction losses and maximize detection probability. As the beam waist increases, the detection probability curve becomes steeper and exhibits more pronounced changes in slope, eventually reaching a smooth saturation zone. In scenarios where the propagation distance is relatively short, a smaller beam width of VAVB can result in a higher detection probability of the signal OAM mode. This is because a smaller beam width allows for a tighter confinement of the signal OAM mode, which can help to reduce the degree of diffraction and increase the probability of detection. However, as the signal propagates over longer distances, the smaller beam width of VAVB can also lead to a higher degree of diffraction, which can cause the signal to spread out and decrease the detection probability of the signal OAM mode. In this case, a larger beam width of VAVB can be more effective in maintaining a higher detection probability of the signal OAM mode, as it allows for a wider confinement of the signal OAM mode and reduces the degree of diffraction. Additionally, the detection probability is higher for VAVBs with larger wavelengths (corresponding to smaller wave numbers). This suggests that VAVBs with larger wave numbers experience reduced

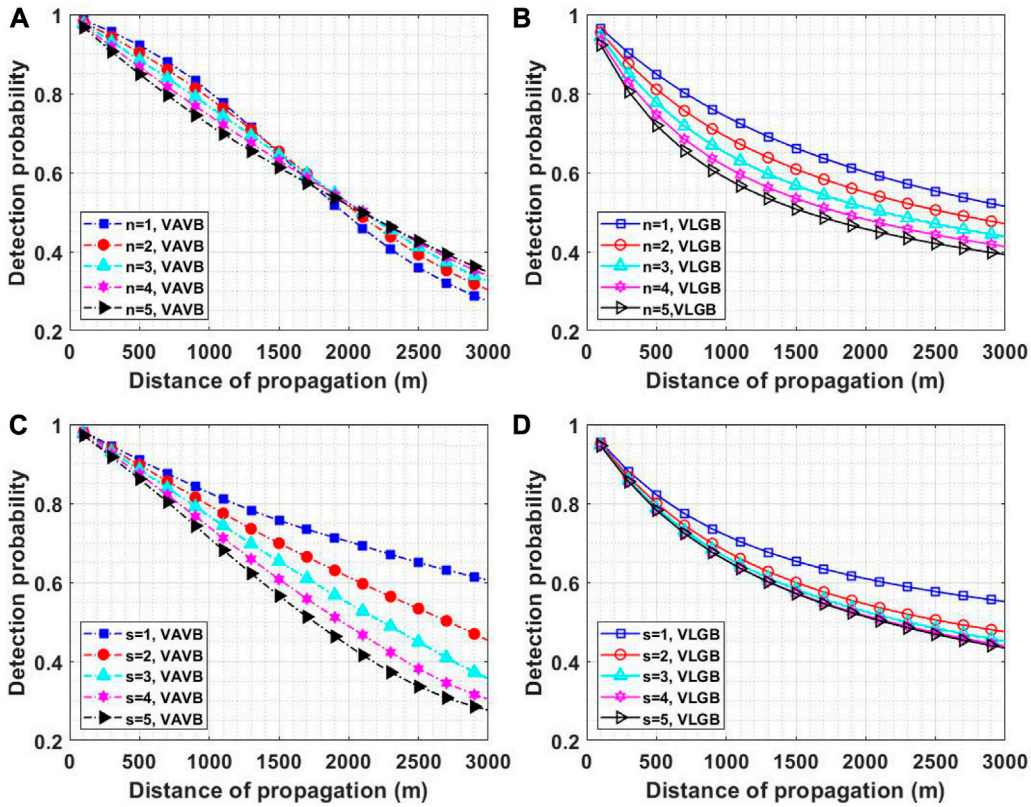

FIGURE 3
Detection probability of the signal OAM for the propagated VAVB through maritime atmospheric turbulence with beam order n **(A,B)** and quantum number s **(C,D)** along the propagation distance z. **(A,C)** and **(B,D)** adopt VAVB and VLGB as the source, respectively.

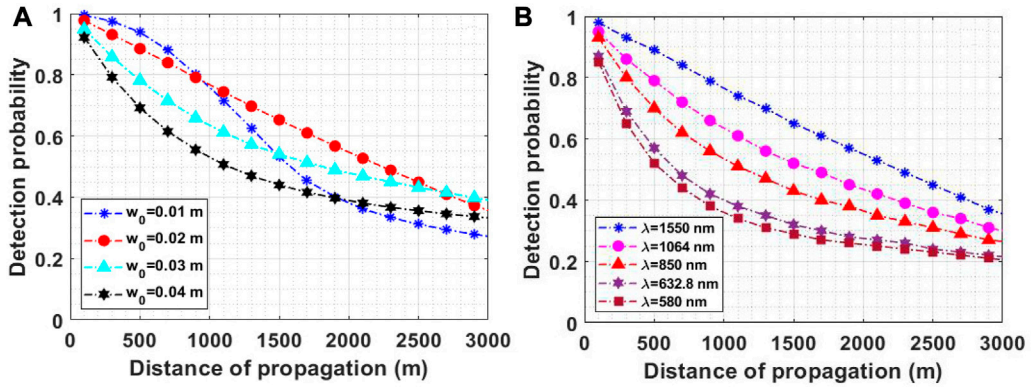

FIGURE 4
Detection probability of propagated vector anomalous vortex beams through maritime atmospheric turbulence with beam width w_0 **(A)** and wavelength λ **(B)** along the propagation distance z.

turbulence effects, while those with smaller wave numbers encounter more turbulence effects.

To clarify, Figure 5 shows the effect of the inner and outer scales of maritime atmospheric turbulence on the detection probability of the signal OAM mode. The figure illustrates that larger values of the inner scale correspond to higher signal OAM mode detection probabilities. This is because larger inner scale eddies in turbulence correspond to fewer turbulence eddies, and hence the signal OAM mode experiences less diffraction. Conversely, the signal OAM mode detection probability decreases as the inner scale sizes decrease, indicating that the OAM mode experiences more diffraction due to the increasing turbulence eddies. These

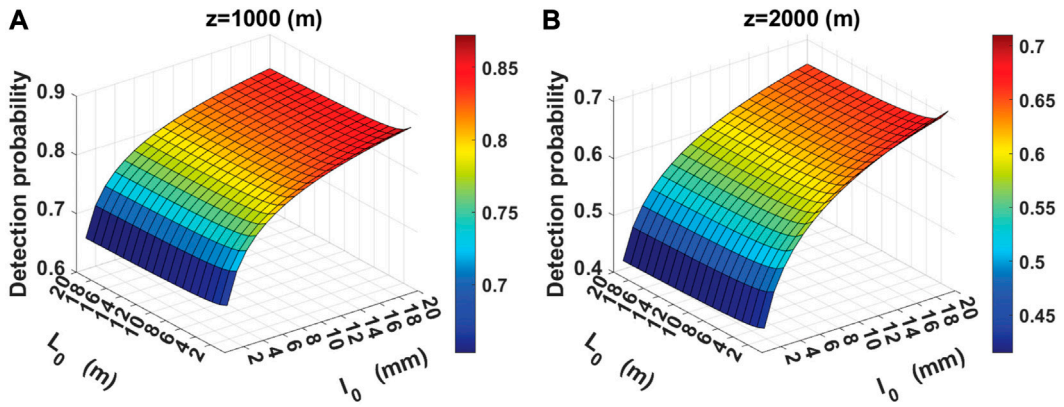

FIGURE 5
Signal OAM detection probability of the signal OAM for propagated vector anomalous vortex beam through maritime atmospheric turbulence versus the outer scale L_0 and the inner scale l_0 of maritime atmospheric turbulence at z = 1000 m **(A)** and z = 2000 m **(B)**.

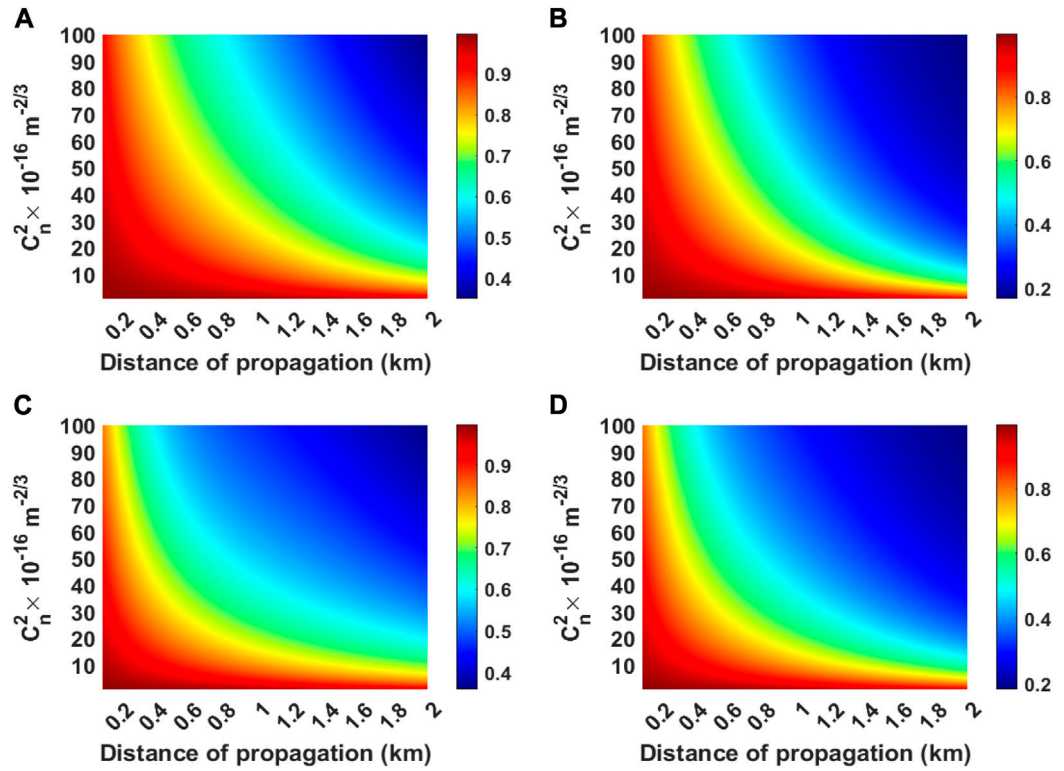

FIGURE 6
Signal OAM detection probability of the signal OAM for propagated vector anomalous vortex beams through maritime atmospheric turbulence versus C_n^2 and propagation distance z for s = 1 & n = 1 **(A)**, s = 3 & n =1 **(B)**, s = 1 & n = 3 **(C)** and s = 3 & n = 3 **(D)**.

results can also be interpreted as a larger inner scale size implying a smaller κ_0 value and less maritime atmospheric turbulence effects. The outer scale of turbulence has a relatively small effect on the detection probability compared to the inner scale, there is a slight decrease in the signal OAM detection probability as the outer scale increases from 1 to 3 m with a constant inner scal. Beyond this range, the effects of the outer scale can be neglected. This can be understood as larger outer scales having similar effects to those that are large enough to cause reflection on the propagated beam Yong et al. [39]. These effects are consistent with the increasing receiver plane distance, which leads to a general reduction in the signal OAM mode detection probability. This is because greater distances entail more maritime atmospheric turbulence.

Figure 6 illustrates the behavior of the detection probability of the received signal OAM mode as a function of the refractive index structure constant and the propagation distance, considering

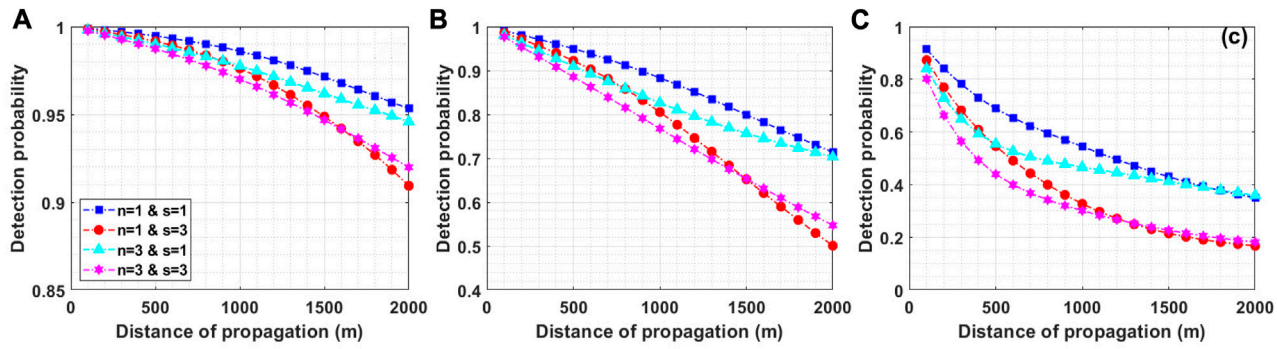

FIGURE 7
Signal OAM detection probability of the signal OAM for the propagated VAVB through maritime atmospheric turbulence *versus* the propagation distance z for $C_n^2 = 1 \times 10^{-16} m^{-3/2}$ **(A)**, $1 \times 10^{-15} m^{-3/2}$ **(B)** and $1 \times 10^{-14} m^{-3/2}$ **(C)**.

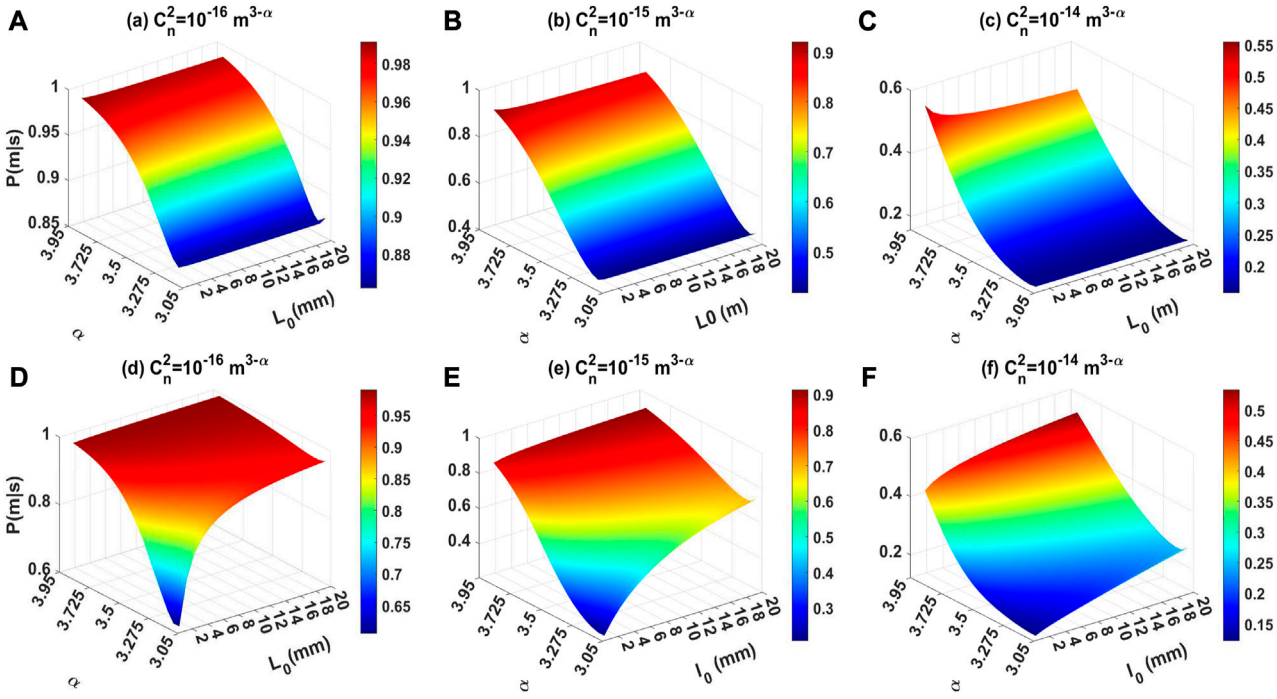

FIGURE 8
Detection probability of the signal OAM for propagated vector anomalous vortex beams through maritime atmospheric turbulence *versus* α with L_0 **(A–C)** and l_0 **(D–F)**.

different values of the beam order (n) and quantum number (s). It is observed that a high signal OAM detection probability can be achieved with weak maritime atmospheric turbulence and a short propagation distance. In the case of weak maritime atmospheric turbulence, a high detection probability is attainable even with a long propagation distance for various values of both the beam order and quantum number, as shown in Figures 6A–D. VAVBs with smaller beam orders exhibit higher detection probabilities at short distances compared to VAVBs with higher beam order, as demonstrated in Figures 6, 7. On the other hand, high beam orders and low quantum numbers yield high signal OAM detection probabilities at long distances, and these differences depend on the strength of the turbulence. Furthermore, it can be observed that the decrease in signal OAM detection probability occurs more rapidly in strong maritime atmospheric turbulence, as depicted in Figure 6C. This indicates that low beam order VAVBs are only preferable for short distances, while high beam order VAVBs are more suitable for long distances.

To investigate the impact of non-Kolmogorov maritime atmospheric turbulence on VAVB's OAM mode, the behavior of the detection probability of the signal OAM mode is analyzed in relation to the non-Kolmogorov parameter (α) with inner and outer scales of maritime atmospheric turbulence, as depicted in Figure 8. It is observed that the variation of the non-Kolmogorov parameter has

a significant influence on the received signal OAM mode. In weak maritime atmospheric turbulence, there is a notable increase in the detection probability with increasing α, reaching a saturation point when $\alpha = 3.55$, as shown in Figures 8A, D. As α approaches 3, a slight increase in the detection probability is observed from its minimum value at $\alpha = 3.1$. However, in the case of moderate and strong maritime atmospheric turbulence, the detection probability decreases as the outer scale increases and the inner scale decreases. This is due to the fact that both humidity and temperature play a role in the refractivity spectrum of maritime atmospheric turbulence. Figures 8D, F demonstrate that the detection probability sharply decreases to its lowest value when the inner scale sizes approach 1 mm. This is because the inner scale sizes in maritime atmospheric turbulence are typically in the range of 1–2 mm. The decreasing detection probability is a consequence of the effect of these small scales on the propagation of the OAM mode in the turbulent medium. The detection probability of the signal OAM mode is significantly affected by the non-Kolmogorov parameter, with different behaviors observed in weak, moderate, and strong maritime atmospheric turbulence. In particular, weak maritime atmospheric turbulence shows an increase in the detection probability with increasing α, while moderate and strong turbulence exhibit a decrease in the detection probability as the inner scale sizes decrease.

4 Conclusion

To summarize, this study investigated the behavior of the intensity distribution and the signal OAM mode detection probability for VAVBs in maritime atmospheric turbulence. The intensity distribution of VAVBs exhibits self-focusing behavior which makes them useful for applications such as optical sensing and communication. This self-focusing property allows the VAVBs to maintain their profile and improve their performance along the propagation distance. The detection probability of the signal OAM mode was found to be influenced by several factors, including the beam waist, beam order, quantum number, wavelength, and turbulence scales. The signal OAM of VAVBs with high beam orders and low quantum numbers perform better over long distances, indicating that higher-order VAVBs are more suitable for long-distance applications. Changes in humidity and temperature cause fluctuations in the refractive index spectral, making the effects of turbulence scales more prominent. The inner scale size in particular has a significant impact on detection probability, with smaller sizes reducing detection probability. Overall, this study provides insights into the behavior of VAVBs in maritime atmospheric turbulence and highlights their potential for optical sensing and communication in turbulent media. The findings suggest that careful consideration of various parameters is necessary when designing systems based on VAVBs, and the self-focusing property of VAVBs should be leveraged for optimal performance.

Data availability statement

The original contributions presented in the study are included in the article/Supplementary material, further inquiries can be directed to the corresponding authors.

Author contributions

Conceptualization, MC; methodology, SW and YC; investigation, HA-A; resources, LG; writing–original draft preparation, HA-A and MC; writing–review and editing, MC and QC; All authors contributed to the article and approved the submitted version.

Funding

This research was funded by National 111 Center, National Natural Science Foundation of China, grant number U20B2059, 61905186, 62231021, 61901336, and 61621005 and the Fundamental Research for the Central Universities, grant number QTZX22037 and YJS2208.

Conflict of interest

Author QC was employed by the company 504th Institute of China Aerospace Science and Industry Corporation (CASIC).

The remaining authors declare that the research was conducted in the absence of any commercial or financial relationships that could be construed as a potential conflict of interest.

Publisher's note

References

1. Willner AE, Huang H, Yan Y, Ren Y, Ahmed N, Xie G, et al. Optical communications using orbital angular momentum beams. *Adv Opt Photon* (2015) 7: 66–106. doi:10.1364/aop.7.000066

2. Wang J. Advances in communications using optical vortices. *Photon Res* (2016) 4: B14–B28. doi:10.1364/prj.4.000b14

3. Zhu F, Huang S, Shao W, Zhang J, Chen M, Zhang W, et al. Free-space optical communication link using perfect vortex beams carrying orbital angular momentum (oam). *Opt Commun* (2017) 396:50–7. doi:10.1016/j.optcom.2017.03.023

4. Al-Amri M, Andrews DL, Babiker M. Structured Light for optical communication *(structured light for optical communication)* (2021).

5. Andrews LC, Phillips RL. Laser beam Propagation through random media *(SPIE)*. 2nd ed. (2005).

6. Cui L. Analysis of marine atmospheric turbulence effects on infrared imaging system by angle of arrival fluctuations. *Infrared Phys Technol* (2015) 68:28–34. doi:10.1016/j.infrared.2014.10.018

7. Cheng M, Guo L, Li J, Yan X, Sun R, You Y. Effects of asymmetry atmospheric eddies on spreading and wander of bessel–Gaussian beams in anisotropic turbulence. *IEEE Photon J* (2018) 10:1–10. doi:10.1109/JPHOT.2018.2842243

8. Zhou Z-L, Xu C-A, Xu H-F, Qu J. Propagation properties of partially coherent crescent-like beams under maritime environment. *J Opt Soc Am A* (2019) 36:1838–45. doi:10.1364/JOSAA.36.001838

9. Gbur G. Partially coherent beam propagation in atmospheric turbulence [Invited]. *J Opt Soc Am A* (2014) 31:2038–45. doi:10.1364/josaa.31.002038

10. Li M, Cvijetic M, Takashima Y, Yu Z. Evaluation of channel capacities of oam-based fso link with real-time wavefront correction by adaptive optics. *Opt Express* (2014) 22:31337–46. doi:10.1364/OE.22.031337

11. Cheng M, Dong K, Shi C, Mohammed A-AHT, Guo L, Yi X, et al. Enhancing performance of air–ground oam communication system utilizing vector vortex beams in the atmosphere. *Photonics* (2023) 10:41. doi:10.3390/photonics10010041

12. Zhao L, Xu Y, Dan Y. Evolution properties of partially coherent radially polarized laguerre–Gaussian vortex beams in an anisotropic turbulent atmosphere. *Opt Express* (2021) 29:34986–5002. doi:10.1364/OE.438743

13. Zhao L, Xu Y, Yang N, Xu Y, Dan Y. Propagation factor of partially coherent radially polarized vortex beams in anisotropic turbulent atmosphere. *J Opt Soc Am A* (2021) 38:1255–63. doi:10.1364/JOSAA.430879

14. Zhao L, Xu Y, Yang S. Statistical properties of partially coherent vector beams propagating through anisotropic atmospheric turbulence. *Optik* (2021) 227:166115. doi:10.1016/j.ijleo.2020.166115

15. Cheng M, Guo L, Zhang Y. Scintillation and aperture averaging for Gaussian beams through non-Kolmogorov maritime atmospheric turbulence channels. *Opt Express* (2015) 23:32606–21. doi:10.1364/OE.23.032606

16. Zhu Y, Zhang Y, Hu Z. Spiral spectrum of airy beams propagation through moderate-to-strong turbulence of maritime atmosphere. *Opt Express* (2016) 24:10847–57. doi:10.1364/OE.24.010847

17. Friehe CA, Larue JC, Champagne FH, Gibson CH, Dreyer GF. Effects of temperature and humidity fluctuations on the optical refractive index in the marine boundary layer. *J Opt Soc America* (1975) 65:1502–11. doi:10.1364/JOSA.65.001502

18. Hill RJ Spectra of fluctuations in refractivity, temperature, humidity, and the temperature-humidity cospectrum in the inertial and dissipation ranges. *Radio Sci* (1978) 13:953–61. doi:10.1029/RS013i006p00953

19. Jellen C, Nelson C, Brownell C, Burkhardt J, Oakley M. Measurement and analysis of atmospheric optical turbulence in a near-maritime environment. *IOP SciNotes* (2020) 1:024006. doi:10.1088/2633-1357/abba45

20. Li Y, Zhang Y. Oam mode of the hankel–bessel vortex beam in weak to strong turbulent link of marine-atmosphere. *Laser Phys* (2017) 27:045201. doi:10.1088/1555-6611/aa5c16

21. Cui X-z, Yin X-l, Chang H, Sun Z-w, Wang Y-j, Tian Q-h, et al. Analysis of the orbital angular momentum spectrum for laguerre–Gaussian beams under moderate-to-strong marine-atmospheric turbulent channels. *Opt Commun* (2018) 426:471–6. doi:10.1016/j.optcom.2018.05.061

22. Yang Y, Dong Y, Zhao C, Cai Y. Generation and propagation of an anomalous vortex beam. *Opt Lett* (2013) 38:5418–21. doi:10.1364/OL.38.005418

23. Ou J, Yin Z, Chi H, Li Q, Yang B, Yang S, et al. Partially coherent anomalous vortex beam in anisotropic turbulence. *Opt Commun* (2023) 537:129411. doi:10.1016/j.optcom.2023.129411

24. Dai Z, Yang Z, Zhang S, Pang Z. Propagation of anomalous vortex beams in strongly nonlocal nonlinear media. *Opt Commun* (2015) 350:19–27. doi:10.1016/j.optcom.2015.03.071

25. Yuan Y, Yang Y. Propagation of anomalous vortex beams through an annular apertured paraxial abcd optical system. *Opt Quan Electron* (2015) 47:2289–97. doi:10.1007/s11082-014-0105-y

26. Dong M, Jiang D, Luo N, Yang Y. Trapping two types of Rayleigh particles using a focused partially coherent anomalous vortex beam. *Appl Phys B* (2019) 125:55–8. doi:10.1007/s00340-019-7165-4

27. Bai Y, Dong M, Zhang M, Yang Y. Properties of a tightly focused circularly polarized anomalous vortex beam and its optical forces on trapped nanoparticles. *Nanoscale Res Lett* (2019) 14:252–7. doi:10.1186/s11671-019-3089-5

28. Li F, Lui H, Ou J. Spiral spectrum of anomalous vortex beams propagating in a weakly turbulent atmosphere. *J Mod Opt* (2020) 67:501–6. doi:10.1080/09500340.2020.1758815

29. Xu Y, Dan Y. Statistical properties of electromagnetic anomalous vortex beam with orbital angular momentum in atmospheric turbulence. *Optik* (2019) 179:654–64. doi:10.1016/j.ijleo.2018.10.194

30. Zhu Y, Chen M, Zhang Y, Li Y. Propagation of the oam mode carried by partially coherent modified bessel–Gaussian beams in an anisotropic non-Kolmogorov marine atmosphere. *J Opt Soc Am A* (2016) 33:2277–83. doi:10.1364/JOSAA.33.002277

31. Huang X, Chang Z, Zhao Y, Wang Y, Zhu X, Zhang P. Generation of the anomalous vortex beam by spiral axicon implemented on spatial light modulator. *Front Phys* (2022) 10:570. doi:10.3389/fphy.2022.951516

32. Zhang Q, Liu Z, Wang X. Generation and characteristics of an airy vortex beam from the anomalous vortex beam. *Results Phys* (2022) 35:105389. doi:10.1016/j.rinp.2022.105389

33. Moreno I, Davis JA, Ruiz I, Cottrell DM. Decomposition of radially and azimuthally polarized beams using a circular-polarization and vortex-sensing diffraction grating. *Opt Express* (2010) 18:7173–83. doi:10.1364/OE.18.007173

34. Yuan Y, Xiao X, Liu D, Fu P, Qu J, Gbur G, et al. Protective consumption behavior under smog: Using a data-driven dynamic bayesian network. *Waves in Random and Complex Media* (2022) 0:1–19. doi:10.1007/s10668-022-02875-6

35. Paterson C. Atmospheric turbulence and orbital angular momentum of single photons for optical communication. *Phys Rev Lett* (2005) 94:153901. doi:10.1103/physrevlett.94.153901

36. Xue B, Cui L, Xue W, Bai X, Zhou F. Generalized modified atmospheric spectral model for optical wave propagating through non-Kolmogorov turbulence. *J Opt Soc Am A* (2011) 28:912–6. doi:10.1364/JOSAA.28.000912

37. Arfken GB, Weber HJ, Harris FE. *Mathematical methods for physicists: A comprehensive guide*. 7th ed. Elsevier (2013).

38. Gradshteyn IS, Ryzhik IM. *Table of integrals, series and products*. seventh edn: Academic Press (2007).

39. Yong K, Tang S, Yang X, Zhang R. Propagation characteristics of a ring airy vortex beam in slant atmospheric turbulence. *J Opt Soc America, B. Opt Phys* (2021) 38:1510–7. doi:10.1364/josab.419348